



Norwegian University of  
Science and Technology

# Conversion of solid reacting particles in a non-premixed double shear layer

**Patrycja Dominika Zareba**

Master of Energy and Environmental Engineering

Submission date: August 2018

Supervisor: Nils Erland L Haugen, EPT

Co-supervisor: Tian Li, EPT  
Andrzej Szlek, Silesian University of Technology

Norwegian University of Science and Technology  
Department of Energy and Process Engineering



## MASTER'S THESIS

---

# Conversion of solid reacting particles in a non-premixed double shear layer

---

*Author:*

Patrycja ZAREBA

*Supervisor at NTNU:*

Nils Erland L. HAUGEN

*Supervisor at SUT:*

Andrzej SZŁEK

*Co-Supervisor at NTNU:*

Tian LI



Norwegian University of Science and Technology  
Faculty of Engineering Science and Technology  
Department of Energy and Process Engineering



Silesian University of Technology  
Faculty of Energy and Environmental Engineering  
Institute of Thermal Technology

Trondheim, June 2018



*Grzecz*, dnia *02.08.2018*  
*Patrycja Łyba*  
(imię i nazwisko studenta)

*270412*  
(nr albumu)

*Energetyka*  
(kierunek studiów)

*Stacjonarne II stopnia*  
(profil, poziom i forma studiów)

### OŚWIADCZENIE

Świadomy/a odpowiedzialności karnej oświadczam, że przedkładana praca magisterska/projekt inżynierski na temat:

*Conversion of solid reacting particles in  
a non-premixed double shear layer*

została napisana przeze mnie samodzielnie.

Jednocześnie oświadczam, że ww. praca :

- nie narusza praw autorskich w rozumieniu ustawy z dnia 4 lutego 1994 roku o prawie autorskim i prawach pokrewnych (j.t. Dz. U. z 2016 r. poz. 666, z późn. zm.) oraz dobór osobistych chronionych prawem cywilnym, a także nie zawiera danych i informacji, które uzyskałem/am w sposób niedozwolony,
- nie była wcześniej podstawą żadnej innej urzędowej procedury związanej z nadawaniem dyplomów wyższej uczelni lub tytułów zawodowych,
- nie zawiera fragmentów dokumentów kopiowanych z innych źródeł bez wyraźnego zaznaczenia i podania źródła,
- złożona w postaci elektronicznej jest tożsama z pracą złożoną w formie pisemnej.

*Patrycja Łyba*  
(podpis studenta)

\* podkreślić właściwe



EPT-M-2018-111

**MASTER THESIS**

for

Student Patrycja Zareba  
Spring 2018**Conversion of solid reacting particles in a non-premixed double shear layer****Background and objective**

In light of a stronger emphasis on increasing the efficiency of combustion processes, which results in a reduction of economic costs but also in reduced emissions of harmful substances, a fundamental understanding of the combustion process is required. During the last years, the effect of turbulence on the conversion rate of solid reacting particles has been studied extensively in premixed mode, i.e. when particles and oxidizer are mixed before reactions start. This is a valid approach for many applications, but there are also a number of applications where particles and oxidizer are NOT perfectly mixed before they start reacting. This situation has not previously been studied and this will be the topic of the current master thesis.

The direct numerical simulation (DNS) tool known as the Pencil-Code will be used to simulate a double shear jet with reacting particles. The double shear jet test case is a classical test case that is commonly used for gas phase combustion. It should also be very useful for solid phase combustion, which nobody has done yet. The reason why the DNS approach was chosen is its ability to resolve the smallest scales of the fluid flow. The LES and RANS approaches, however, have to model these smallest scales, and their results therefore rely on the accuracy of the models.

Some simplifications have to be made in order to make the computational costs affordable. The main simplifications made in this work are: 1) the particles will not affect the momentum of the fluid and 2) they will have a constant radius, i.e.; they will not be influenced by the reactant. Also, 3) the reactions will take place on the particles surface, 4) they will be infinitely fast and 5) neither endothermic nor exothermic. Finally, 6) the Reynolds number will be kept low.

This study will provide a better insight into the particle mixing and cluster formation processes. Through this, it will be useful for predicting the behaviour in e.g. pulverized coal burners.

The work of this Master thesis is linked to the Gaspro project (NFR FP project 267916)

**The following tasks are to be considered:**

1. Literature review on the effect of turbulence on reactive particles.
2. Learning how to use the Pencil-Code
3. Numerical simulations of the double shear jet with non-reacting particles in 2D
4. Numerical simulations of the double shear jet with reacting particles in 2D
5. Numerical simulations of the double shear jet with reacting particles in 3D
6. Data processing and analysis of results.
7. Summary and final conclusions.
8. Make proposal for further work
9. Write the master thesis

-- " --

Within 14 days of receiving the written text on the master thesis, the candidate shall submit a research plan for his project to the department.

When the thesis is evaluated, emphasis is put on processing of the results, and that they are presented in tabular and/or graphic form in a clear manner, and that they are analysed carefully.

The thesis should be formulated as a research report with summary both in English and Polish, conclusion, literature references, table of contents etc. During the preparation of the text, the candidate should make an effort to produce a well-structured and easily readable report. In order to ease the evaluation of the thesis, it is important that the cross-references are correct. In the making of the report, strong emphasis should be placed on both a thorough discussion of the results and an orderly presentation.

The candidate is requested to initiate and keep close contact with his/her academic supervisor(s) throughout the working period. The candidate must follow the rules and regulations of NTNU as well as passive directions given by the Department of Energy and Process Engineering.

Risk assessment of the candidate's work shall be carried out according to the department's procedures. The risk assessment must be documented and included as part of the final report. Events related to the candidate's work adversely affecting the health, safety or security, must be documented and included as part of the final report. If the documentation on risk assessment represents a large number of pages, the full version is to be submitted electronically to the supervisor and an excerpt is included in the report.

Pursuant to "Regulations concerning the supplementary provisions to the technology study program/Master of Science" at NTNU §20, the Department reserves the permission to utilize all the results and data for teaching and research purposes as well as in future publications.



The final report is to be submitted digitally in DAIM. An executive summary of the thesis including title, student's name, supervisor's name, year, department name, and NTNU's logo and name, shall be submitted to the department as a separate pdf file. Based on an agreement with the supervisor, the final report and other material and documents may be given to the supervisor in digital format.

Department of Energy and Process Engineering, March 1<sup>st</sup> 2018

Prof. Nils Erland L Haugen  
Academic Supervisor  
e-mail: [nilshau@ntnu.no](mailto:nilshau@ntnu.no)



Tian Li  
Co-supervisor  
Postdoktor





## Abstract

As the increasing the efficiency of the combustion processes is crucial nowadays, a fundamental understanding of this process is required. This thesis is focusing on the effect of turbulence on the conversion rate of solid reacting particles in non-premixed mode. The DNS tool, the Pencil-Code is used to simulate a double shear jet with reacting particles, in order to resolve the smallest scales of the fluid flow. In this study, the reaction rate turned out to not to change linearly with increasing number of particles. The results showed that for Stokes number equal to 0.35 the particles created the sharpest clusters affecting the reaction rate. The necessity of future work on the subject is underlined, i.e. implementation of the realistic chemistry of the combustion process, further analysis for increasing number of particles and performing presented simulations with a different method such as LES, in order to compare the results and computational cost to the accuracy of the results ratio.

## **Acknowledgements**

The work of this Master thesis has been compiled under the aegis of the Norwegian University of Technology in Trondheim, benefiting from the expert knowledge of prof. Nils Erland L Haugen and dr Tian Li, with support from mgr Ewa Karchniwy. The thesis also enjoys the patronage of prof. Andrzej Szlęk from the Silesian University of Technology in Gliwice.



# Contents

<b>List of Figures</b>	<b>vi</b>
<b>1 Introduction</b>	<b>1</b>
1.1 Aim of the thesis . . . . .	1
1.2 Objectives . . . . .	1
<b>2 Modeling</b>	<b>2</b>
2.1 Initial conditions . . . . .	2
2.2 Equations . . . . .	4
2.3 2D case . . . . .	6
2.4 3D case . . . . .	17
<b>3 Summary</b>	<b>31</b>

## List of Figures

1	The domain . . . . .	3
2	Plot presenting initial profile . . . . .	7
3	The rate of reactant consumption depending on the particle diameter and density in 2D . . . . .	8
4	Snap shots presenting particles flow in 2D case for densities $10^3, 10^4$ and $10^5 \frac{kg}{m^3}$ respectively, for times between $3.46 \cdot 10^{-5}s$ and $5.35 \cdot 10^{-4}$ with regular timestep . . . . .	9
5	Snap shots presenting reactant flow in 2D case for densities $10^3, 10^4$ and $10^5 \frac{kg}{m^3}$ respectively, for times between $3.46 \cdot 10^{-5}s$ and $5.35 \cdot 10^{-4}$ with regular timestep . . . . .	10
6	Snapshots presenting particles, vorticity and reactant consumption in 2D case for density $10^4 \frac{kg}{m^3}$ . . . . .	11
7	Plot presenting average mean square fluid velocity in X direction for 2D case. . . . .	12
8	Plots presenting average particle numbers and fitting Gaussian distribution in X direction for 2D case for densities $10^3, 10^4$ and $10^5 \frac{kg}{m^3}$ respectively . . . . .	14
9	Plot presenting average reactant fraction in X direction for 2D case for densities $10^3, 10^4$ and $10^5 \frac{kg}{m^3}$ respectively . . . . .	15
10	Plot presenting width of reactant distribution with time for 2D case, for all presented densities . . . . .	16
11	Plot presenting width of particle distribution with time for 2D case, for all presented densities . . . . .	16
12	Plot presenting $f$ as defined in eq. 26 for 2D case for $10^4 kg/m^3$ . . . . .	17
13	The rate of reactant consumption depending on the particle diameter and density in 3D for $10^6$ particles . . . . .	18
14	Plot presenting comparison of the reactant density decay for different densities and particle numbers, with fitting tangential dashed lines. . . . .	19
15	Decay rate for different densities and particles amount . . . . .	20
16	Plot presenting average mean square fluid velocity in X direction for 3D case . . . . .	20
17	Snap shots presenting particles flow in 3D case for densities $10^3, 10^4$ and $10^5 \frac{kg}{m^3}$ respectively for $10^6$ particles . . . . .	22
18	Snap shots presenting particles flow in 3D case for densities $10^3, 10^4$ and $10^5 \frac{kg}{m^3}$ respectively for $10^6$ particles . . . . .	23
19	Snap shots presenting vorticity and reactant consumption in 3D case for density $10^4 \frac{kg}{m^3}$ and $10^6$ particles . . . . .	24

20	Figure shows snapshots for particles flow for density $10^4 kg/m^3$ for different particles amount . . . . .	25
21	Figure shows snapshots for reactant flow for density $10^4 kg/m^3$ for different particles amount . . . . .	26
22	Comparison of particle densities in X direction for 3D case for different densities and amount of particles respectively 1, 4 and 8 millions. . . . .	27
23	Comparison of averaged reactant fraction in X direction for 3D case for different densities and amount of particles respectively 1, 4 and 8 milions. . . . .	28
24	Plot presenting width of reactant within time for 3D case, for all presented densities . . . . .	29
25	Plot presenting width of particles location within time for 3D case, for all presented densities . . . . .	30
26	Plot presenting particles clustering for 3D case for different densities and particles amount . . . . .	30





# 1 Introduction

## 1.1 Aim of the thesis

Despite the fact that fossil-fueled power plants are criticized by environmentalists, it cannot be disregarded that the technology of energy production from renewable sources (RES) is still not living up to societies expectations and needs, as it is not stable. Stability and constancy are the biggest advantages of the fossil fuels, and until the renewable sources will be able to satisfy this need, the majority of the energy system will still be based on gas and coal.

Simultaneously with the development of RES technologies, the fossil fuels combustion process is improved, in order to satisfy the standards regarding the conditions of pollutant emission. One of the ways to achieve it is to increase the efficiency of the whole thermodynamic cycle, in which the combustion process remains the most unknown and complicated. In order to improve it, it is essential to understand how the process works at small scales. So far in terms of numerical simulations of the coal combustion, analyses were focusing on emissions of harmful substances and NO formation [1]. As stated in Hawkes et. al [2], for non-premixed combustion, efficient mixing is essential. The article though is focused on molecular mixing in gas combustion, which is well analyzed in the variety of cases, i.e. in Dinesh et. al [3]. The point of this thesis is to analyze the effects of turbulence on the non-premixed char combustion process. The results may be relevant for power plants with pulverized coal burners, as there are plenty of applications where particles and oxidizer are not mixed perfectly before the reaction occurs. This case has not been previously studied, as more attention was devoted to the situation where fuel and reactant were premixed, although the necessity of it was already highlighted and began in Kruger et. al [4].

## 1.2 Objectives

Numerical methods were well known as soon as analytics were applied in order to describe and solve physical phenomena. With the first computers, the first numerical analyzes were performed and they have turned out to be extremely useful tools. Within years, the optimization analyzes of the processes were going further and further, and as a result, increasingly detailed analyzes have to be done.

In order to find numerical solutions, different approaches may be applied. The Reynolds-averaged Navier–Stokes (RANS) models are time-averaged.

This method requires modelling nearly all scales of the solution - only mean quantities are computed directly. The results are describing the statistics, not the physics of the flow. RANS approach faces difficulties predicting important aspects of reactive flows [5].

Large Eddy Simulations (LES) method is more exact but is spatial filtering, so only the turbulent fluctuations above a particular size are solved directly with the Navier-Stokes equations - the small scale eddies are modelled. The explanation for this is the assumption that the smaller turbulent eddies are isotropic, so they always behave in predictable and similar ways, irrespective of the turbulent flow field.

In the Direct Numerical Simulation (DNS) the N-S system of equations is solved directly [6] with refined meshes capable of resolving all turbulence length scales, including the Kolmogorov microscale [7]. It leads to a large number of computational unknowns. It requires fully three-dimensional grids and an enormous amount of CPU time - this is why the calculations had to be performed on the supercomputer (Stallo) located at the University of Tromsø.

For all the simulations presented in this work, the Pencil Code (PC) [8] tool, written in Fortran 95, is used. The PC development was started in 2001 by Axel Brandenburg and Wolfgang Dobler [9], and primarily was designed to deal with weakly compressible turbulent flows. It is designed for efficient computation with massive parallelization and to achieve it, explicit finite differences are used. Its modular structure enables users to apply a large variety of physical setups, therefore users and developers are from various branches of science.

## 2 Modeling

### 2.1 Initial conditions

A double shear layer test case is commonly used for non-premixed combustion of gas. An example can be found in Ansys page [10]. The presented analyzes are made for a particular domain taken from the L case in the article by Hawkes et al. [2] which can be seen in Figure 1a. Its size is  $12H$  in the stream-wise direction ( $x$ -axis),  $14H$  in the transverse direction ( $y$ -axis) and  $8H$  in the span-wise direction ( $z$ -axis). The  $H$  parameter equals  $0.72\text{mm}$ .

The middle layer (jet), which height is given by  $H$ , is filled with reacting particles embedded in an inert gas (B). The other layers of the domain consist

of reactant (A). The characteristic jet velocity is  $U$ , equal to  $72m/s$ . The characteristic Mach number equals 0.16 and is given by the equation

$$M = \frac{U}{c_a} \quad (1)$$

where  $c_a$  is the sound speed in the air stream. The cold flow Reynolds number of the jet can be calculated by:

$$Re_{jet} = \frac{UH}{\nu_a} \quad (2)$$

$\nu_a$  is kinematic viscosity of the air. The initial width of the air jet is defined by:

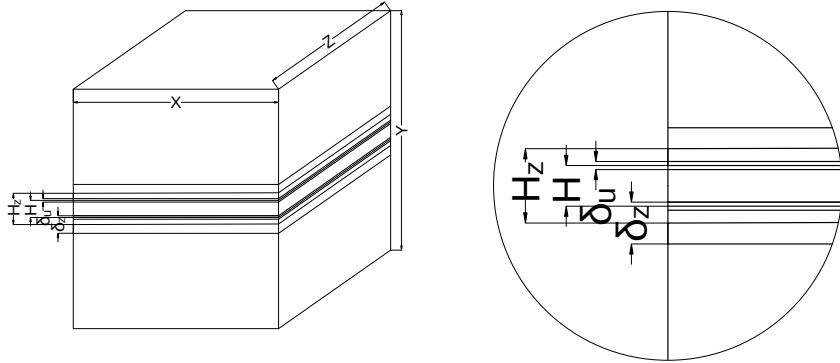
$$H_z = H - \delta_u + \delta_z \quad (3)$$

where  $\delta_z$  is 0.74mm and is the initial thickness of the mixture fraction variation, and  $\delta_u$  is the initial velocity shear layer thickness and can be calculated as:

$$\delta_u = \frac{H}{5} \quad (4)$$

In order to initialize the shear-generated turbulence, a weak white noise is superimposed on the mean velocity field.

The case does not include gravity, and all the boundaries in the domain are periodic.



(a) Sketch presenting whole domain

(b) Enlargement of the domain

Figure 1: The domain

## 2.2 Equations

The Pencil Code solves the fluid equations [11] using a sixth-order finite difference scheme for spatial discretization and a third-order Runge–Kutta scheme for temporal discretization. The code treats the particles as Lagrangian point particles, which interact with the gas phase through the drag force. The particles are spherical and are treated as point particles, as their size (diameter equal to  $5 \cdot 10^{-7}m$ ) is significantly smaller than the grid. The friction force with which particles affect the gas is ignored. The density of the gas phase is equal to 1.

The equation solved are analogical to Haugen et al. [13]. The continuity equation is solved as

$$\frac{D\rho}{Dt} = -\rho \nabla \cdot \mathbf{u}, \quad (5)$$

where  $\rho$  is density,  $\mathbf{u}$  is the fluid velocity,  $t$  is time and  $D/Dt = \delta/\delta t + \mathbf{u} \cdot \nabla$  is the convective derivative. The momentum equation is given by

$$\rho \frac{D\mathbf{u}}{Dt} = \nabla \tau + \rho \mathbf{f} + \mathbf{F}, \quad (6)$$

where  $\mathbf{f}$  is the tension force,  $\mathbf{F}$  is the drag force and  $\tau$  is the viscous stress which is defined as

$$\tau = 2\rho \mathbf{S} \quad (7)$$

where  $\mathbf{S} = (1/2)(\delta u_i/\delta x_j + \delta u_j/\delta x_i) - (1/3)\sigma_{ij}\nabla \cdot \mathbf{u}$  is the traceless rate of strain tensor.

The equation of motion of the reactant is described as

$$\frac{\delta X}{\delta t} + \mathbf{u} \cdot \nabla X = D\nabla^2 X + \tilde{R}, \quad (8)$$

where  $X$  is the mole fraction of reactant and  $\tilde{R}$  is the sink term representing the reaction of reactant on the surface of the particles.

The motion of the  $i$ th particle is given by

$$\frac{d\mathbf{r}^i}{dt} = \mathbf{V}^i \quad (9)$$

and the velocity is given by

$$\frac{d\mathbf{V}^i}{dt} = \mathbf{a}^i \quad (10)$$

where the particle acceleration caused by fluid drag force is calculated as

$$\mathbf{a}^i = \frac{u_{rel}^i}{\tau_t}. \quad (11)$$

The particle response time  $\tau_t$  is equal to

$$\tau_t = \frac{\tau_p}{1 + f_c^i} \quad (12)$$

where  $\tau_p$  is given by equation 15, and the Reynolds number correction is  $f_c^i = 0.15(Re_p^i)^{0.687}$ .  $Re_p$  is the particle Reynolds number, calculated for the relative velocity between the particles and the fluid  $u_{rel}^i$ , and for characteristic linear dimension equal to particle diameter, just as given in 2.

The Stokes numbers were calculated as following

$$St = \frac{\tau_l}{\tau_p} \quad (13)$$

where

$$\tau_l = \frac{H}{U} \quad (14)$$

and

$$\tau_p = \frac{\rho_p d_p^2}{18v_a}. \quad (15)$$

The dimensionless Damköhler number, which relates the chemical reaction timescale to the transport phenomena rate, and is given by:

$$Da = \frac{\tau_l}{\tau_c} \quad (16)$$

where  $\tau_l$  was given in equation 14, and the chemical reaction timescale  $\tau_c$  is calculated as

$$\tau_c = \frac{1}{\alpha} \quad (17)$$

and the reactant consumption rate [12] is defined as

$$\alpha = n_p A_p \kappa \quad (18)$$

where  $n_p$  is the particle number density,  $A_p$  is the particles surface area, and  $\kappa$  is the mass transfer coefficient, which is calculated as

$$\kappa = \frac{ShD}{d_p} \quad (19)$$

where diffusivity  $D$  equals  $10^{-4}m^2s^{-1}$  and  $Sh$  is the Sherwood number, given by the Ranz-Marshall Correlation

$$Sh = 2 + 0.69Re_p^{\frac{1}{2}}Sc^{\frac{1}{3}} \quad (20)$$

and  $Sc$  is the Schmidt number

$$Sc = \frac{v}{D}. \quad (21)$$

The heterogeneous reaction is assumed to be immediate, and neither endothermic nor exothermic. Calculations are made for simple reaction, where the reactant is consumed at the surface of particles, though it does not affect the particle mass and diameter. Hence, there is no direct correlation between the density of the particles and the reaction rate. The reaction can be written as



such that the reactive term from equation 8 is described as

$$\tilde{R} = \frac{1}{V_{cell}} \sum_i A_p^i \kappa X_\infty^i. \quad (23)$$

The  $X_\infty^i = X(\mathbf{r}^i)$  gives information about the far field reactant mole fraction, which is set equal to the reactant mole fraction of the fluid cell where the particle is.

### 2.3 2D case

In order to reduce the required computational costs, the first simulations were performed in a 2D domain. The span-wise direction ( $z - axis$ ) was established as non-existing, except so-called ghost points. This allowed the calculations to be done with the P.C., and to calculate i.e. cells volume. The initial profile of the jet is shown in Figure 2. The grid is dependent on the dimensions of the domain. The number of grid points across  $H$  is 24, and its resolution is equal in each direction.

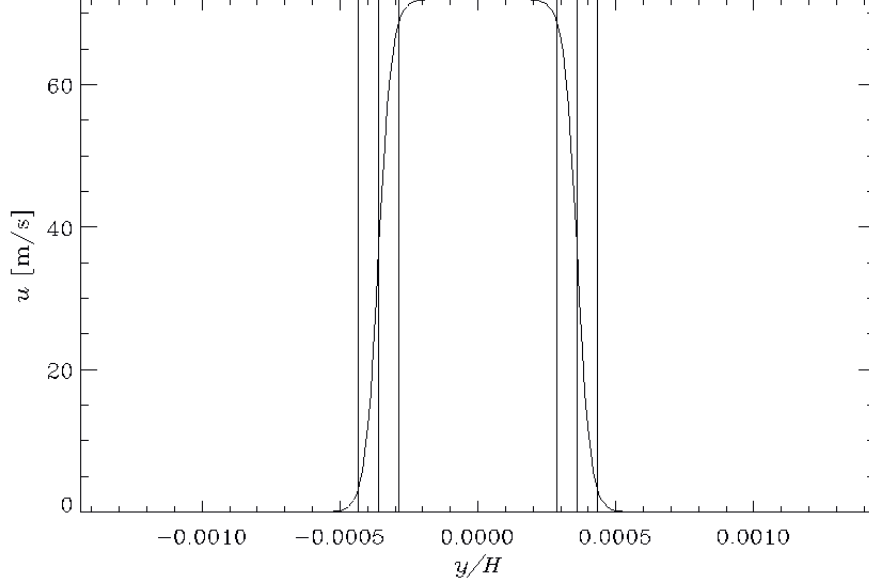


Figure 2: Plot presenting initial profile

The amount of particles is  $10^3$  and is kept like this for all the 2D simulations. Their initial velocity is equal to the velocity of the fluid. The kinematic viscosity of the fluid is equal to  $2 \cdot 10^{-5} m^2 s^{-1}$ , which gives a Reynolds number of 2592. The influence of their density is visible when it comes to clustering and following the eddies. This relation is presented in the Fig. 3.

What is clearly visible from the Fig. 3 is that for smaller particles (diameter equal to  $10^{-7}$ ) the difference in reactant decay (equation 23) for various particles densities is insignificant. In order to increase the reactant consumption, bigger particles were required, as the reaction depends on the size of a particle. Also, between the Stokes number and the diameter of the particles is a quadratic dependence, while linear with their density. Firstly, for increasing density, it can be seen that the decay is increasing. This occurs until a certain point, for density  $10^5 kg/m^3$ , then the tendency is reversed. The particle flow is shown in Fig. 4. For the smallest densities, particles follow the fluid, while creating small and not dense clusters. For the biggest density particles are thrown away from the jet, and the fluid is not able to carry them. As in this case, the mixing is weak, the decay of the reactant is slowing down. In Fig. 5 snapshots of the reactant flow are shown. For the biggest density, the reactant is consumed mostly in the closest surrounding of jet and in later timesteps, it is shown that inside of the eddies there is no



reactant (the colour is dark blue). This is caused by weak mixing.

The case with particle density equal to  $10^4 \frac{kg}{m^3}$  has the Stokes number which is closest to unity. The vorticity and reactant consumption for this case are presented in Fig. 6. The eddies tend to merge and create bigger ones, which is caused by the two-dimensionality. The reactant is marked with colours, where the fraction equal to zero is black, and equal to one is white. This is crucial to recognize it, as the lack of the reactant in the surrounding of clusters in the combustion process can lead to incomplete combustion.

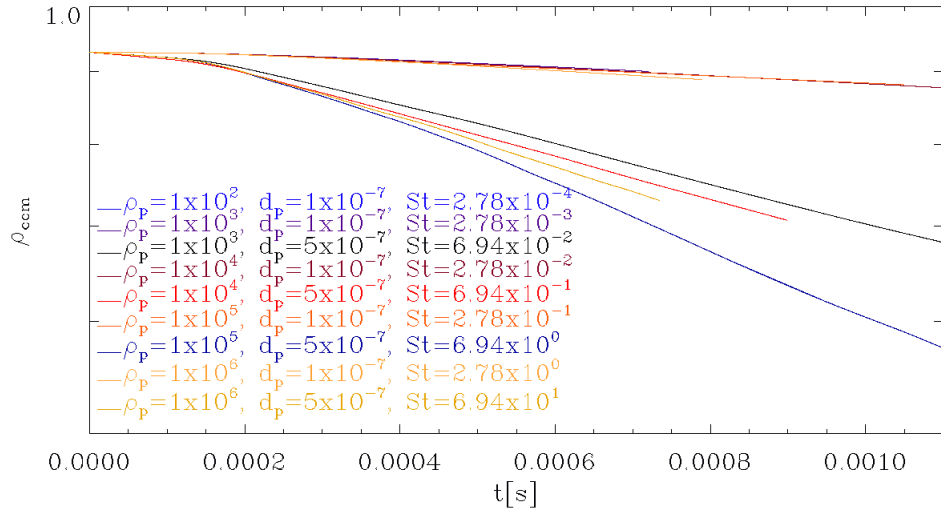


Figure 3: The rate of reactant consumption depending on the particle diameter and density in 2D

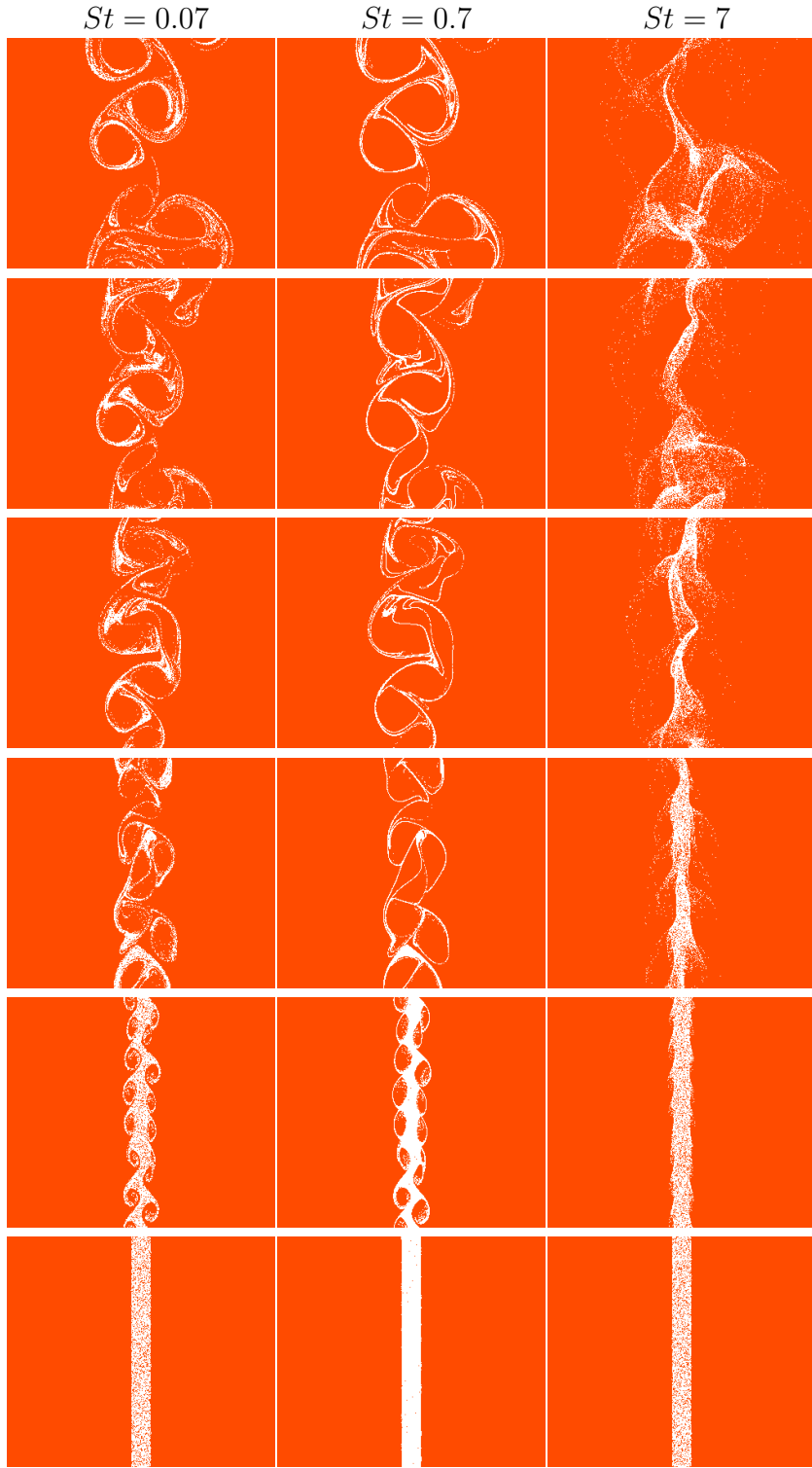


Figure 4: Snap shots presenting particles flow in 2D case for densities  $10^3$ ,  $10^4$  and  $10^5 \frac{kg}{m^3}$  respectively, for times between  $3.46 \cdot 10^{-5} s$  and  $5.35 \cdot 10^{-4}$  with regular timestep

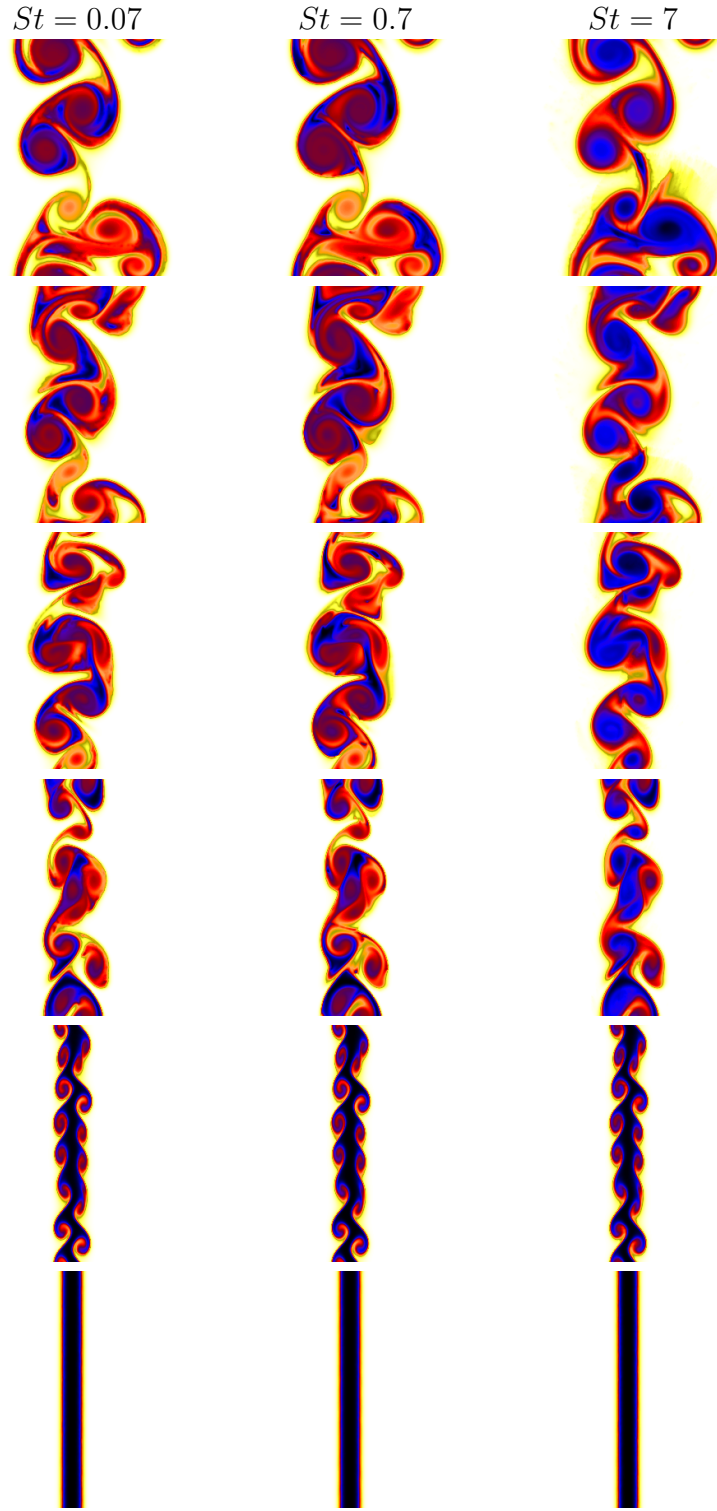


Figure 5: Snap shots presenting reactant flow in 2D case for densities  $10^3$ ,  $10^4$  and  $10^5 \frac{kg}{m^3}$  respectively, for times between  $3.46 \cdot 10^{-5} s$  and  $5.35 \cdot 10^{-4}$  with regular timestep

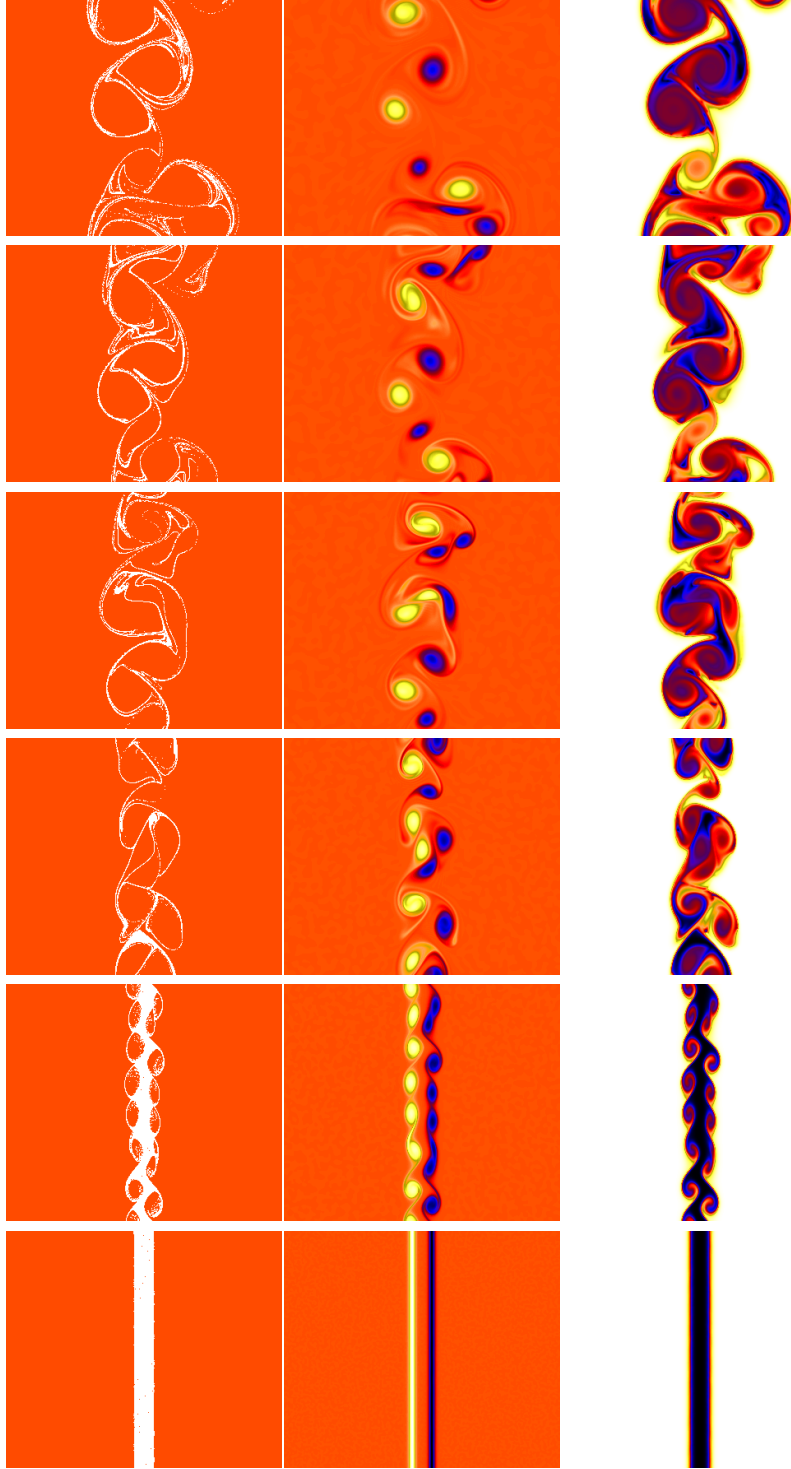


Figure 6: Snapshots presenting particles, vorticity and reactant consumption in 2D case for density  $10^4 \frac{kg}{m^3}$

For all three cases, the velocity of the fluid remains the same, as it does not depend on the particles. The fluid accelerates until approximately 700 m/s and then slows down, and it is shown in Fig. 7. The domain is symmetric but the profiles are not - this is due to the turbulence, as the eddies are spreading randomly.

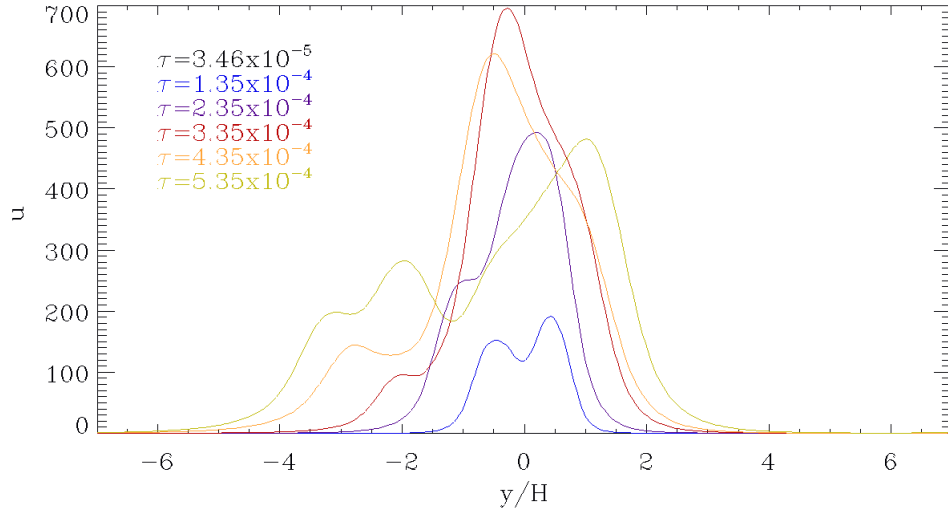


Figure 7: Plot presenting average mean square fluid velocity in X direction for 2D case.

In order to present the jet spreading, the width of particle number density (Fig. 8) and reactant fraction (Fig. 9) is shown for particular times. Thick lines are presenting fitted Gaussians, and thin lines are showing spreading itself. For each time-step, the spreading is defined as a sum of beams where the reactant fraction is below 99% or the particle number density is above approximately 5% of the maximum value. The reason for that is making the charts easier to read and to avoid a situation where even a single particle outside jet would be treated as its enlargement. For particle number density the averaging was made in order to see smoother plots. The data were averaged over 10% of the time-step, which is  $8.3 \cdot 10^{-6}$ s. For densities  $10^3$  and  $10^4 \text{ kg/m}^3$  the spreading tendency for particle density is very similar, for the density of  $10^5 \text{ kg/m}^3$  it spreads the slowest. It does not affect the reactant fraction significantly, for all three cases it looks similar. Within the time, the jet spreads more widely, though it is not fully consumed anywhere. In order to see the general tendency of spreading for chosen time-steps, i.e. for which time-step the jet has the largest width, the Gaussian function was fitted to

the plots. The function is given by

$$f(x) = A_0 e^{\frac{-z^2}{2}} \quad (24)$$

where  $A_0$  is the height of the Gaussian, and

$$z = \frac{x - A_1}{A_2} \quad (25)$$

and  $A_1$  and  $A_2$  are centre of the Gaussian and the width (the standard deviation), respectively. Those coefficients are estimated as the best fit for the given plot.

The differences in spreading are presented in Fig. 10 and Fig. 11. For the Gaussian, the sigma (width) is the ratio of spreading. The cases with smaller densities seem likewise, and the case for density  $10^5 \text{ kg/m}^3$  at first is less spread, at one point though it is overreaching the two others. For Gaussian profiles, it is clear that they do not follow well the tendency of reactant to spread. It starts begins with a smaller value, as the Gaussian is very thin for the first time-step. The shape of reactant distribution is more like an unit step function. It is hard to fit the Gaussian into it, and it is visible in Fig. 10 that the minimum value of this function is below zero. For particle distribution, Gaussians are following the trend better, although the difference increases for later time-steps.

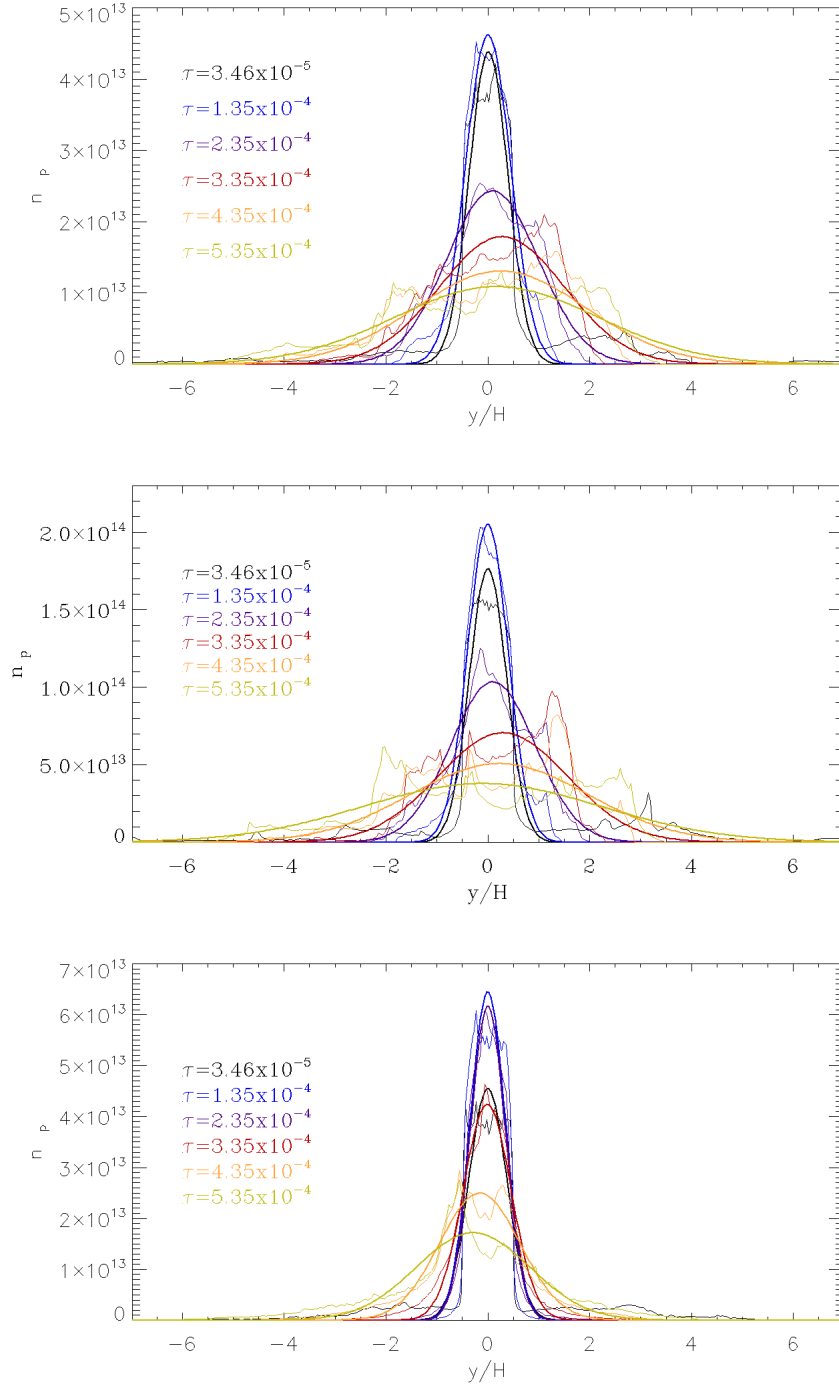


Figure 8: Plots presenting average particle numbers and fitting Gaussian distribution in X direction for 2D case for densities  $10^3, 10^4$  and  $10^5 \frac{kg}{m^3}$  respectively

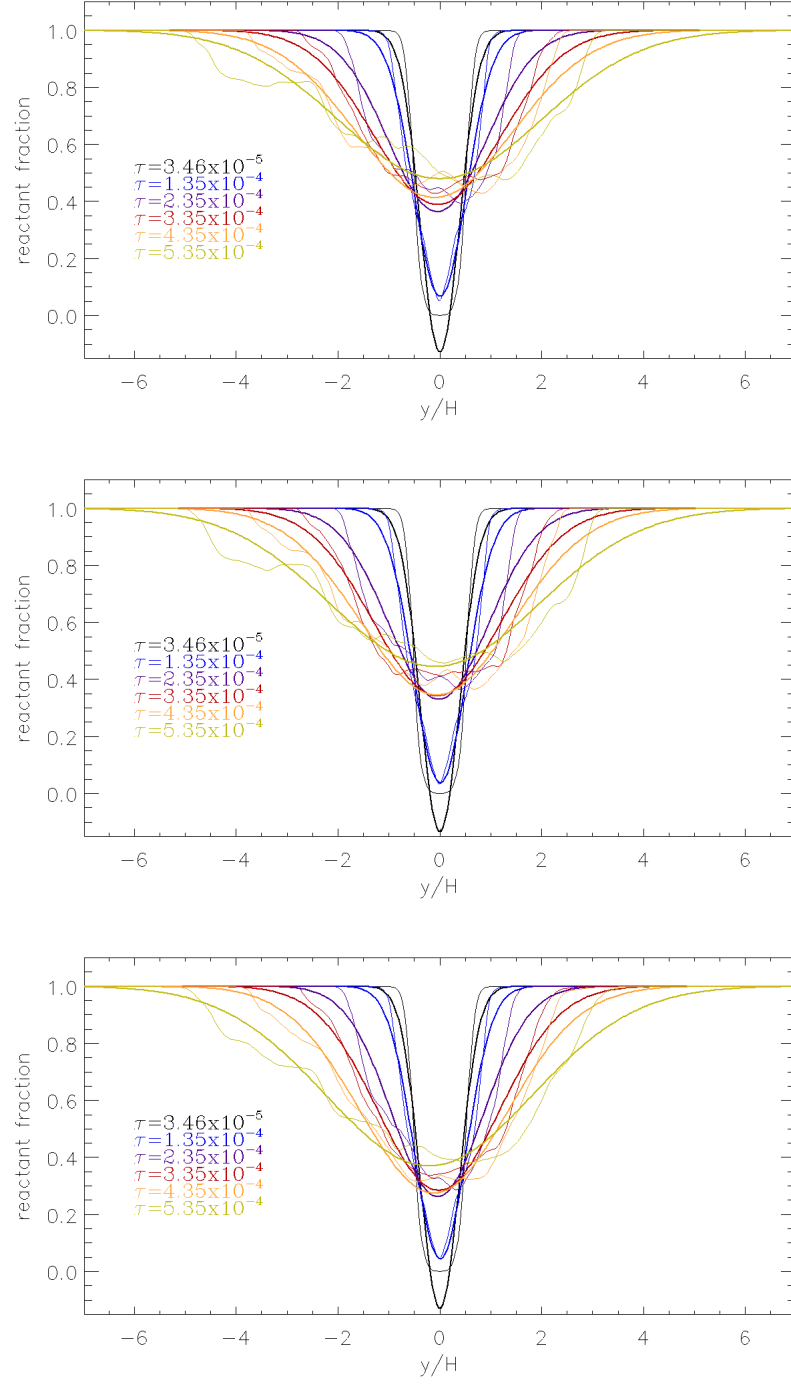


Figure 9: Plot presenting average reactant fraction in X direction for 2D case for densities  $10^3, 10^4$  and  $10^5 \frac{kg}{m^3}$  respectively



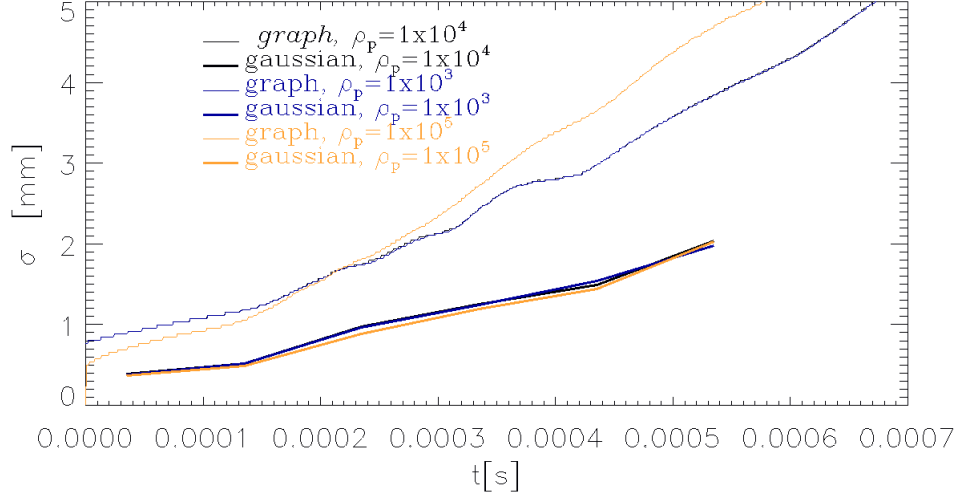


Figure 10: Plot presenting width of reactant distribution with time for 2D case, for all presented densities

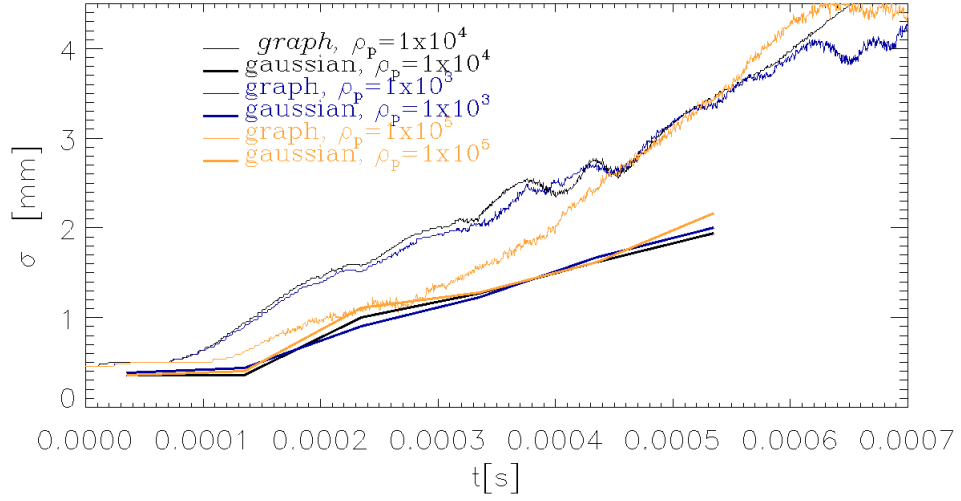


Figure 11: Plot presenting width of particle distribution with time for 2D case, for all presented densities

The tendency of particles to cluster is not obvious to determine. In order to do that, the domain was divided in the stream-wise direction into small pieces, which created beams parallel to the transverse direction. The average

of particle density per beam does not distinguish whether all particles are located one next to another, or they are spread through the whole length of the beam. In order to have a better look on this case, the Fig 12. is presenting the following ratio as a function of time

$$f = \frac{\overline{n_p^2}}{\overline{n_p}^2}. \quad (26)$$

This was calculated for each beam and then averaged over the stream-wise direction. The graph shows the tendency to cluster when the turbulence starts, and it decreases with the simulation progress. Two peaks are visible, and they correspond to third and fifth snapshots from page 11. On those snapshots, the clusters are the sharpest.

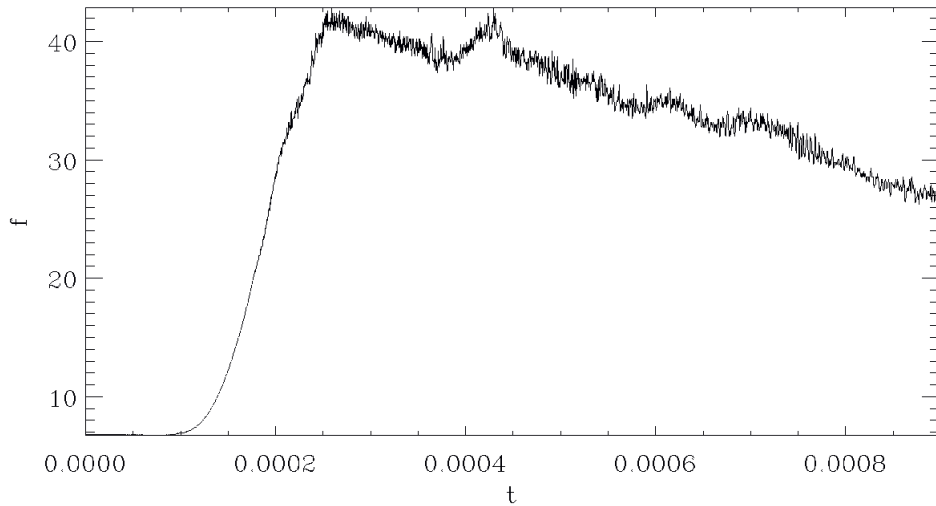


Figure 12: Plot presenting  $f$  as defined in eq. 26 for 2D case for  $10^4 kg/m^3$

## 2.4 3D case

The simulations in 3D were performed for the domain presented in Fig.1a. The number of grid points were 288, 336 and 192 for x, y and z direction, respectively. The kinematic viscosity was equal to  $4 \cdot 10^{-5} m^2 s^{-1}$ , so the Reynolds number was 1296. Initial profile and all rest of the initial parameters were set similarly as for 2D case. First results are given for particle numbers equal to  $10^6$ . It can be seen from Fig 13 that the reactant consumption was rather stable and independent of variations in density. Apparently, the domain was too big, so simulations for more particles were performed.

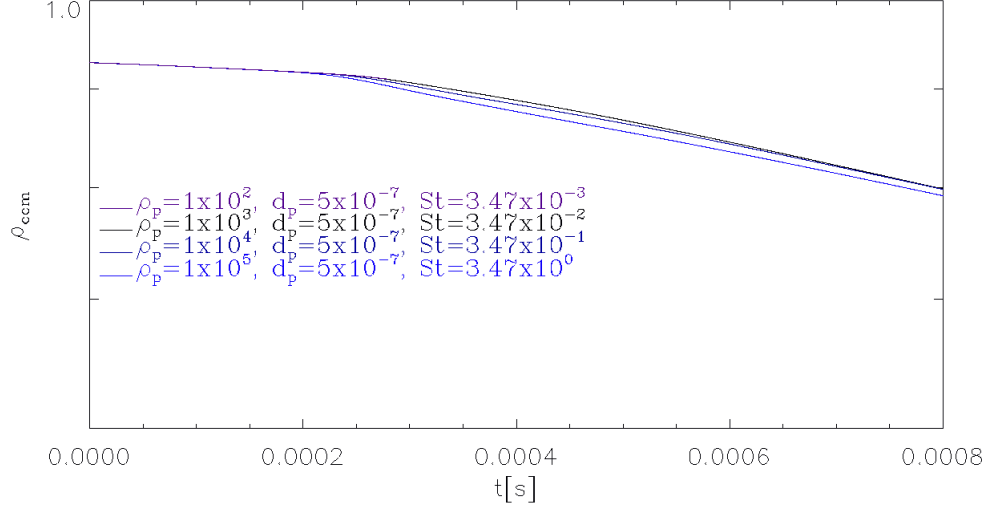


Figure 13: The rate of reactant consumption depending on the particle diameter and density in 3D for  $10^6$  particles

Based on Fig. 14, the decay rate  $\alpha$  was taken from the equation of the line tangential to the plot (dashed lines). The first part of the slope is due to consumption of the reactant in the closest surrounding of the jet, then the turbulence begins to influence on the particles. The values are not fitted perfectly, but it gives the general trends. The numbers of particles increased four and eight times, though the decay rate did not change with the same ratio.

The decay rates for particular densities and particle numbers are presented in Fig. 15. For the densities  $10^3$  and  $10^4 \text{ kg/m}^3$ , the steepness of the slopes decreases with increasing particles amount, while for  $10^5 \text{ kg/m}^3$  it seems to be more linear. For the smallest density, the slope is reaching the plateau area for a smaller number of particles, thus for the biggest density can be predicted that also will behave more logarithmic for bigger particles amount.

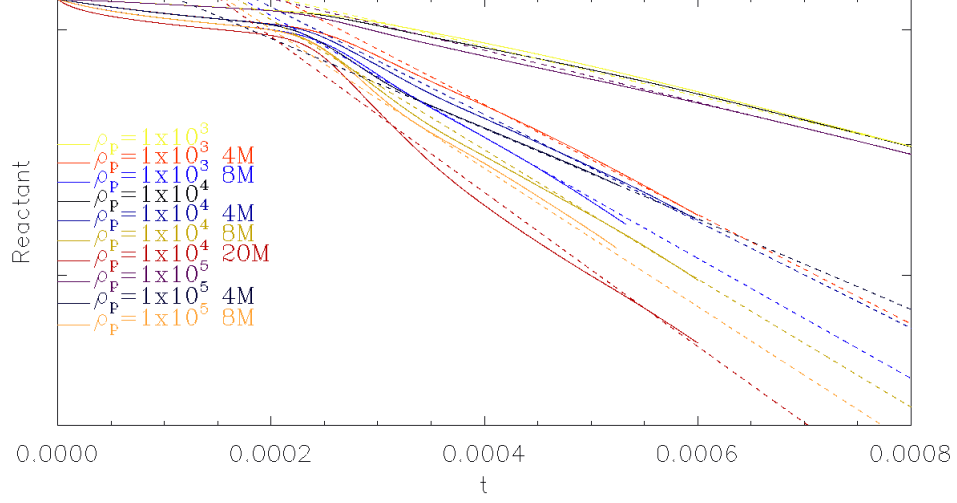


Figure 14: Plot presenting comparison of the reactant density decay for different densities and particle numbers, with fitting tangential dashed lines.

For density  $10^4 \text{ kg/m}^3$ , changing from 1 million to 20 million particles, the decay rate changes only around 4 times. For other densities, particles number is changing from 1 million to 8 million particles. The differences in the decay rate for same densities but varies particle amounts may be mostly caused by mixing. Variations between the same particle numbers for distinct densities have the main cause in clustering of particles. For density  $10^5 \text{ kg/m}^3$ , for 4 million particles the decay rate is the lowest. This is due to the fact, that heavy particles did not follow the eddies, and were longer than in other cases located in the middle of the jet. Then the particles were thrown away from the centre of the domain but still did not follow the fluid well. However, for more particles, this case has the biggest decay rate. Paradoxically, the reason for this is probably the same. While for smaller densities the particles are following the fluid and tend to cluster, in this case, the particles are thrown and do not follow the fluid. As there are more particles, more reactant is consumed.

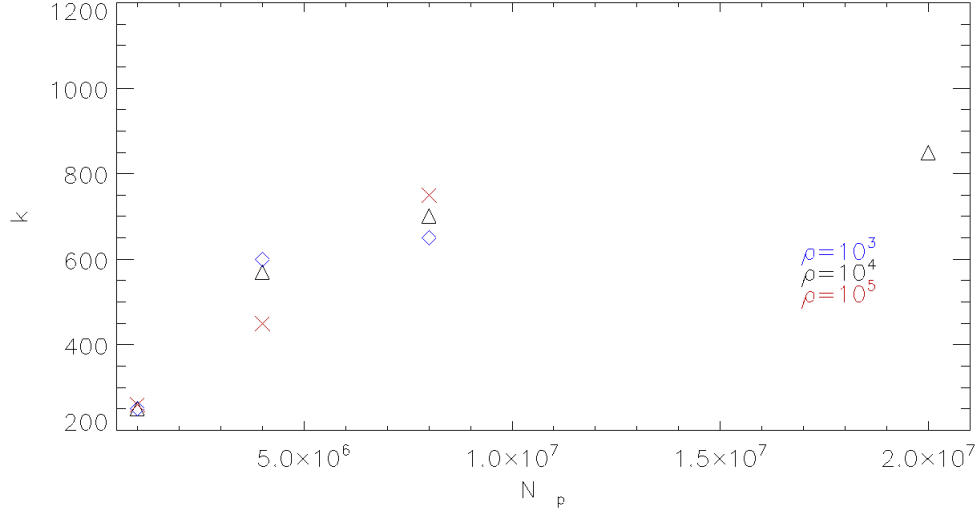


Figure 15: Decay rate for different densities and particles amount

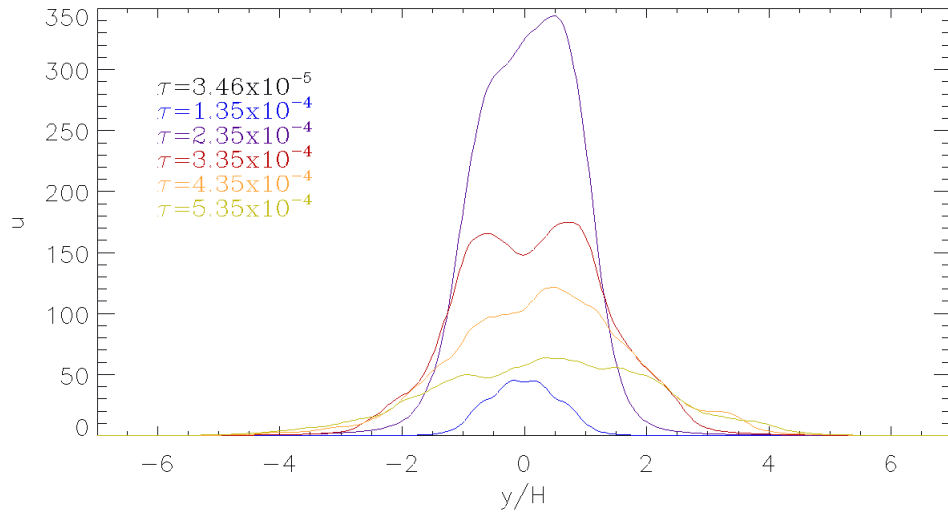


Figure 16: Plot presenting average mean square fluid velocity in X direction for 3D case

The fluid velocity visible in Fig. 16 is approximately twice lower than for 2D case, due to higher viscosity, but the tendency of increasing and decreasing is notably similar. The profiles are more symmetric than in 2D case, as the flow is less turbulent.

Even though the Reynolds number is half of the 2D case, the flow is fully turbulent. Looking at Fig. 17 it can be seen that particle clusters appears at the same density as for 2D case, which is  $10^4 \text{ kg/m}^3$ . Therefore, also for 3D simulations, the focus is on the case with the density of  $10^4$ . Less dense particles are following the vorticity entirely, and the heavier ones are independent of the eddies. In Fig. 18, is shown the influence of this occurrence on the reactant. The colours have the same meaning as for 2D case. The densest particles are consuming most of the reactant in the jet, and it is represented by the blue area. Smaller blue areas are visible also in the middle case - that is due to clustering.

The biggest differences with the 2D case are seen in Fig. 19, in vorticity and reactant fraction. The eddies are breaking down into smaller scales, and the reactant consumption is not as fast as it was for 2D. That proves that in order to analyze the real case, simulations cannot be substituted with 2D, as it ignores the turbulence effect.

In Fig. 20 it is clear that the clusters are identical for 4 and 8 million particles. This is due to the fact that particles are not affecting the fluid flow. The visible difference is seen for 20 million particles, significantly bigger clusters are shown. It may be caused simply by the significantly bigger amount of particles, as overall tendency looks similar. As it is clear in Fig. 21, for this case the reactant in the middle of the jet is consumed almost immediately (as the colour is black). The mixing is not efficient enough to break the clusters and provide more reactant to particles.

Fig. 22 represents the averaged particle number densities for various densities and amount of particles. Unlike the 2D case, no averaging was needed. The sharpest shape of the distribution is in the case of  $\rho = 10^4$ , although this case still looks similar to the first one. For the density  $10^5 \text{ kg/m}^3$  the distribution in second time-step ( $1.35 \cdot 10^{-4} \text{ s}$ ) show how particles concentrate on edges of the jet. The biggest difference is for third time-step ( $2.35 \cdot 10^{-4} \text{ s}$ ), as for density  $10^5 \text{ kg/m}^3$ , majority of particles is still inside the jet, while for other densities it is already spread among the domain. This is due to lack of mixing of heavier particles. What is shown in Fig. 23, the reactant consumption presents more similarities between densities than the previous figure. For 1 million particles all cases are almost identical, within the increase of particles, the case for the density  $10^5 \text{ kg/m}^3$  slightly differs, as it is more smooth for the time-steps. That is due to the fact, that in other cases particles spread widely faster.

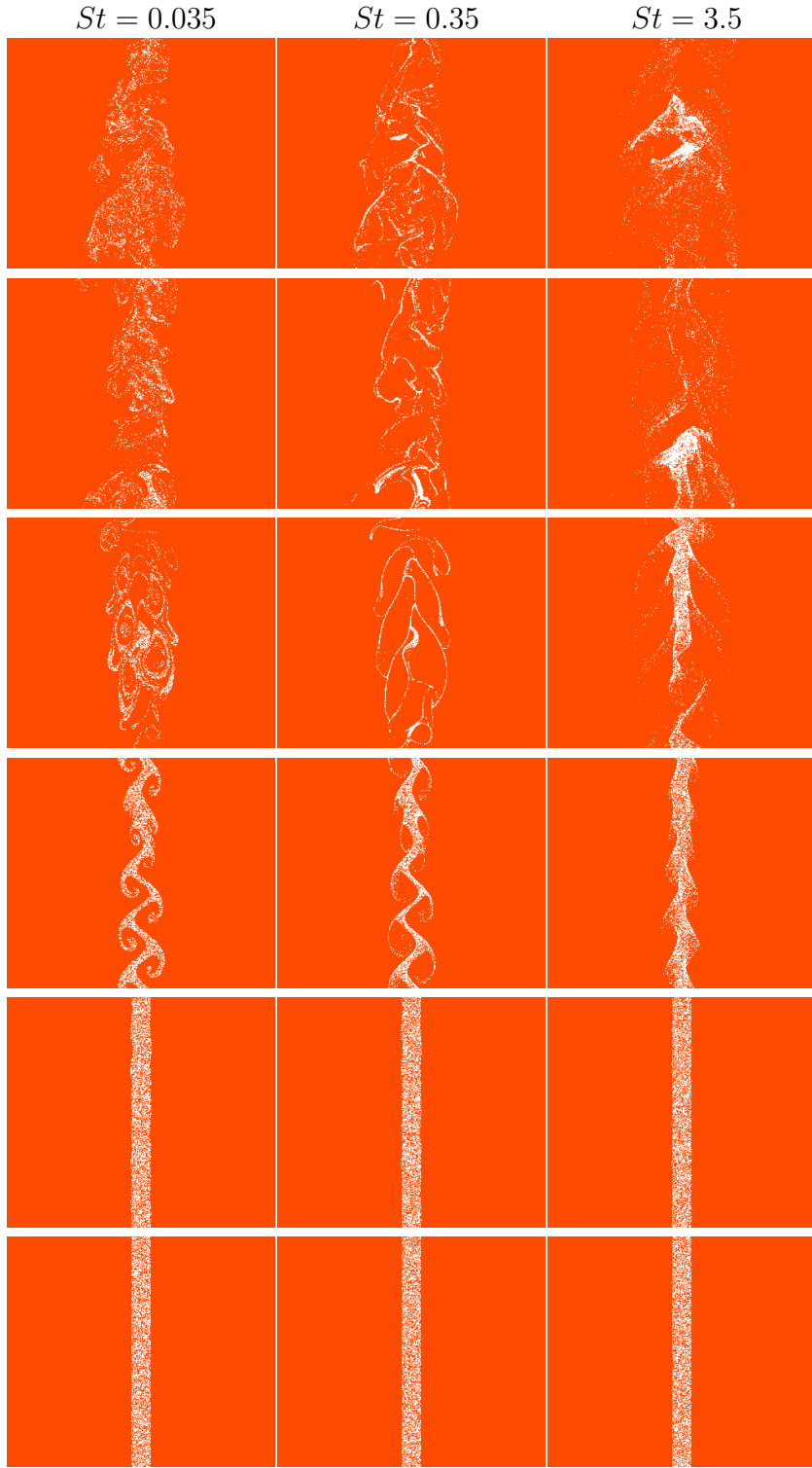


Figure 17: Snap shots presenting particles flow in 3D case for densities  $10^3$ ,  $10^4$  and  $10^5 \frac{kg}{m^3}$  respectively for  $10^6$  particles

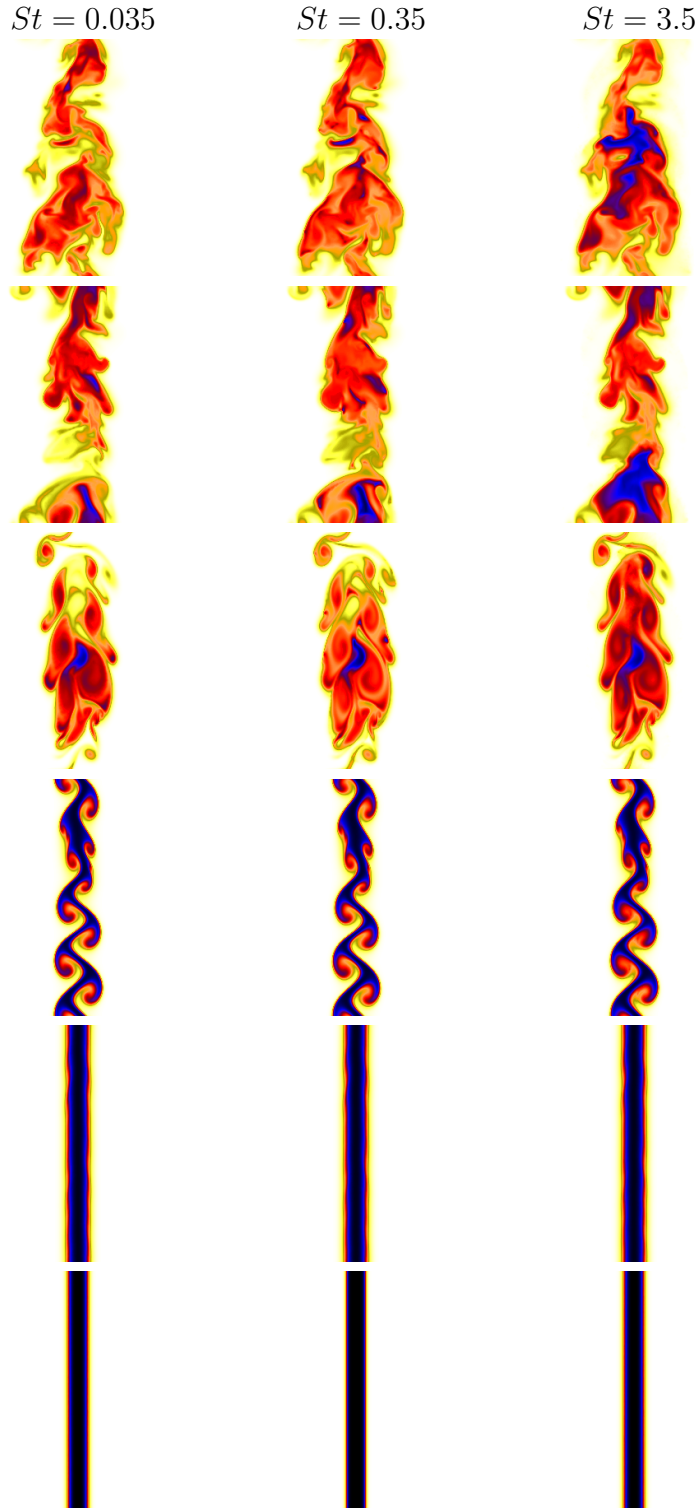


Figure 18: Snap shots presenting particles flow in 3D case for densities  $10^3$ ,  $10^4$  and  $10^5 \frac{kg}{m^3}$  respectively for  $10^6$  particles



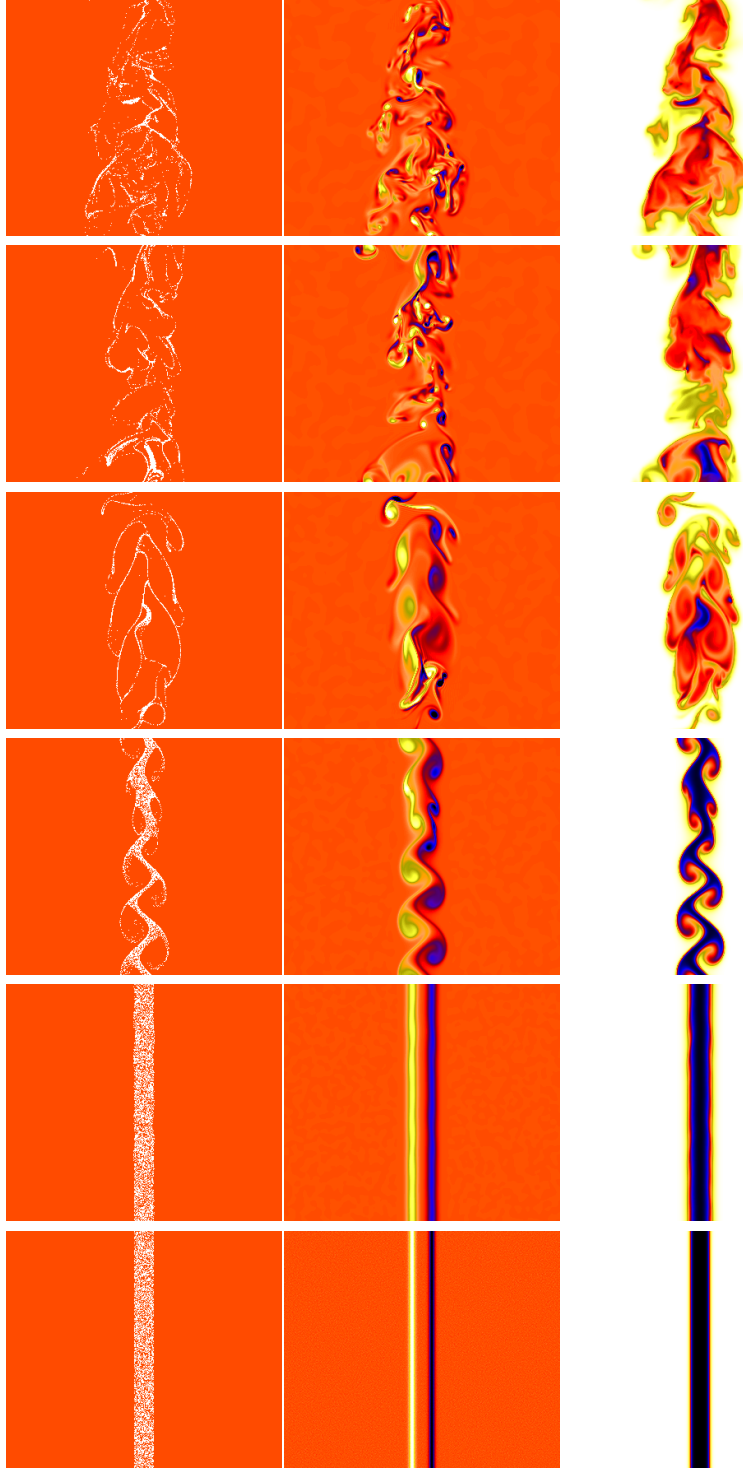


Figure 19: Snap shots presenting vorticity and reactant consumption in 3D case for density  $10^4 \frac{kg}{m^3}$  and  $10^6$  particles

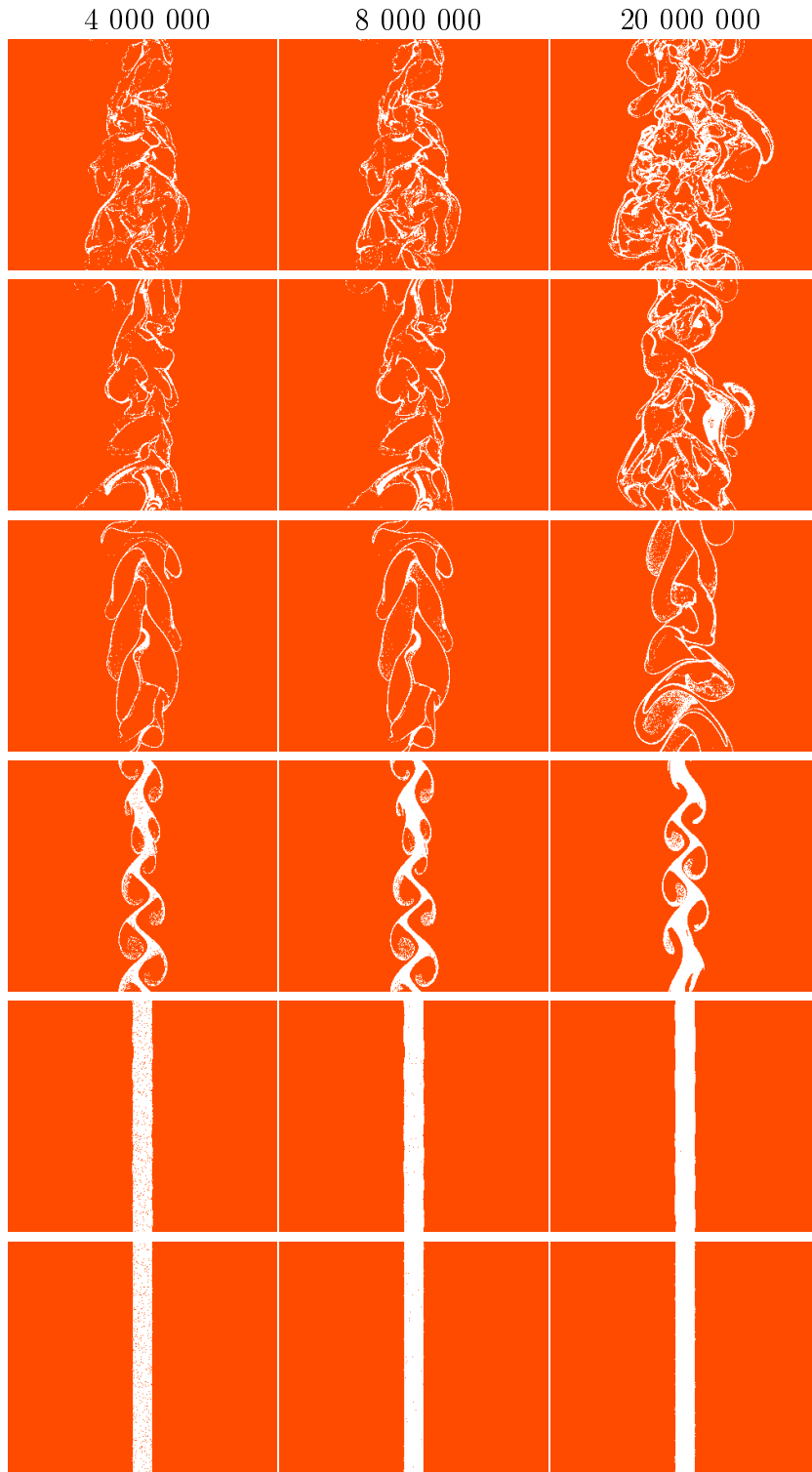


Figure 20: Figure shows snapshots for particles flow for density  $10^4 kg/m^3$  for different particles amount

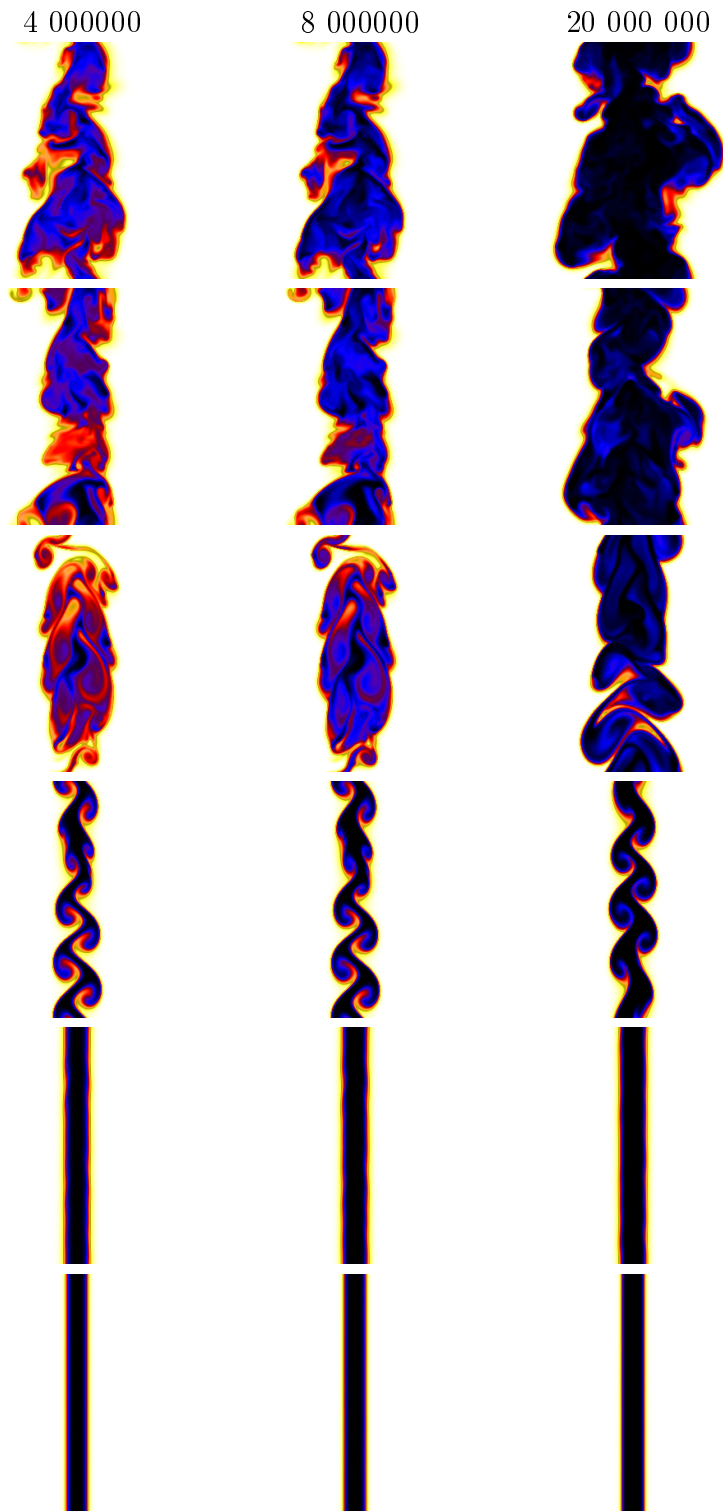


Figure 21: Figure shows snapshots for reactant flow for density  $10^4 kg/m^3$  for different particles amount

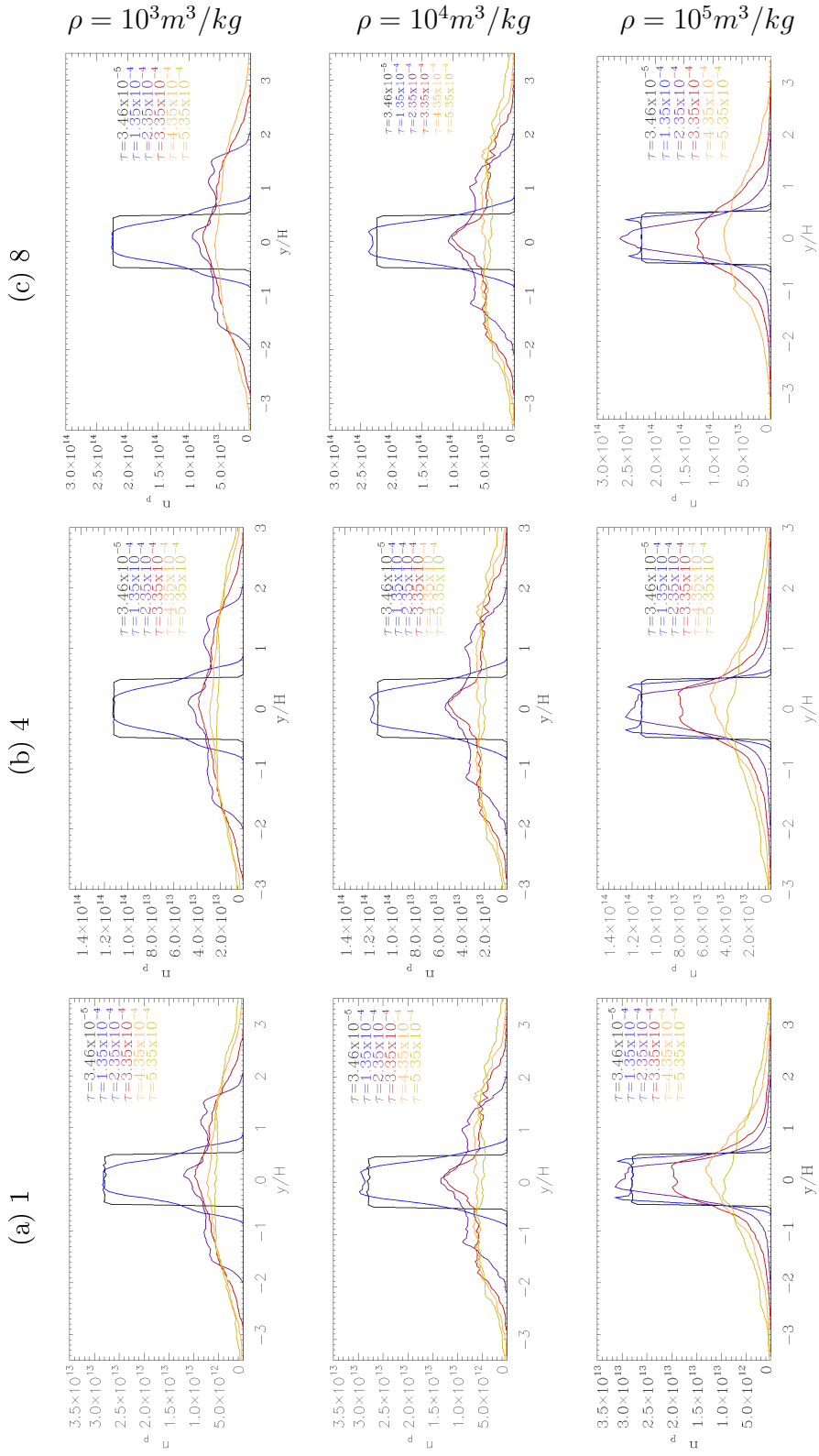


Figure 22: Comparison of particle densities in X direction for 3D case for different densities and amount of particles respectively 1, 4 and 8 millions.

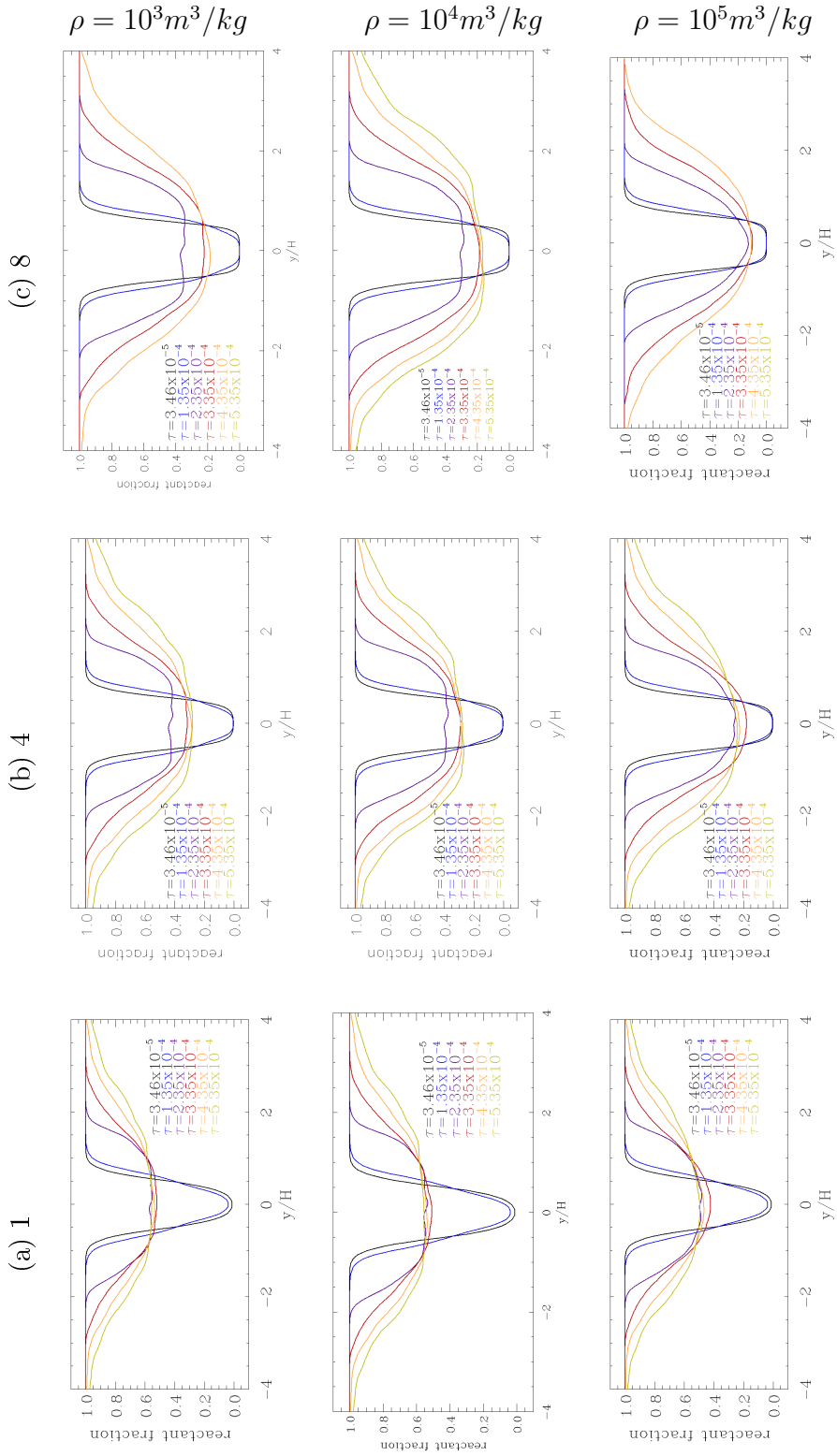


Figure 23: Comparison of averaged reactant fraction in X direction for 3D case for different densities and amount of particles respectively 1, 4 and 8 millions.

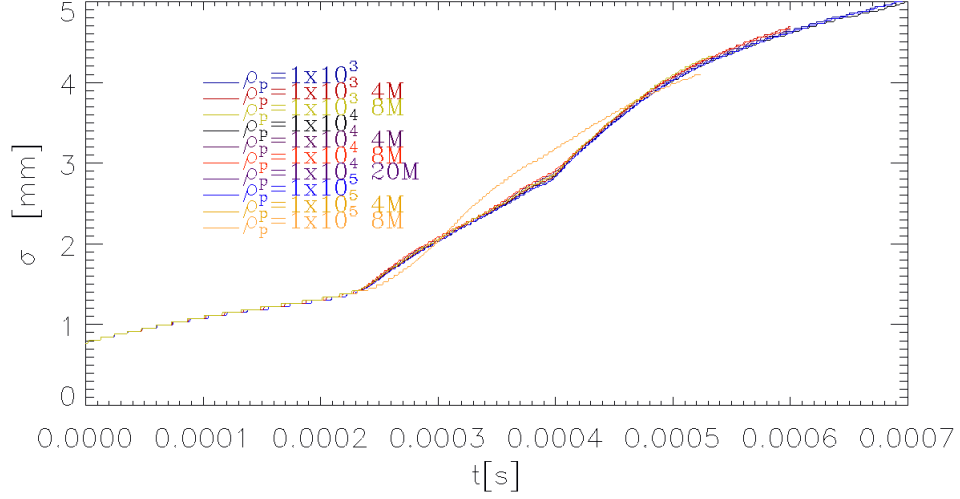


Figure 24: Plot presenting width of reactant within time for 3D case, for all presented densities

The spread of the width of the reactant fraction is shown in Fig. 24. It is independent on the particles, except from one case all slopes are the same. For the 8 millions particles of density  $10^5 kg/m^3$ , dissimilarity is visible. It can be caused by the fact that huge amount of particles were just thrown away from the jet, and then did not follow the eddies, so more reactant far from jet was consumed unrelatedly on the flow.

With Fig. 25 the slopes varies significantly. The wider jet is reached the fastest for 4 million particles for the biggest density, though the growing tendency seems to slow down at the end. This phenomena is probably due to throwing the particles out of the jet. The spreading is slowing down, as the particles after being thrown are not carried by the eddies. The slowest jet spreading is for the same density, but for 1 million particles. For this amount of particles, the spreading is the weakest. The case with 20 millions particles after the first high speed of spreading slows down and follows the case for the same density but 4 million particles, which may be resulting from the clusters which are not breaking.

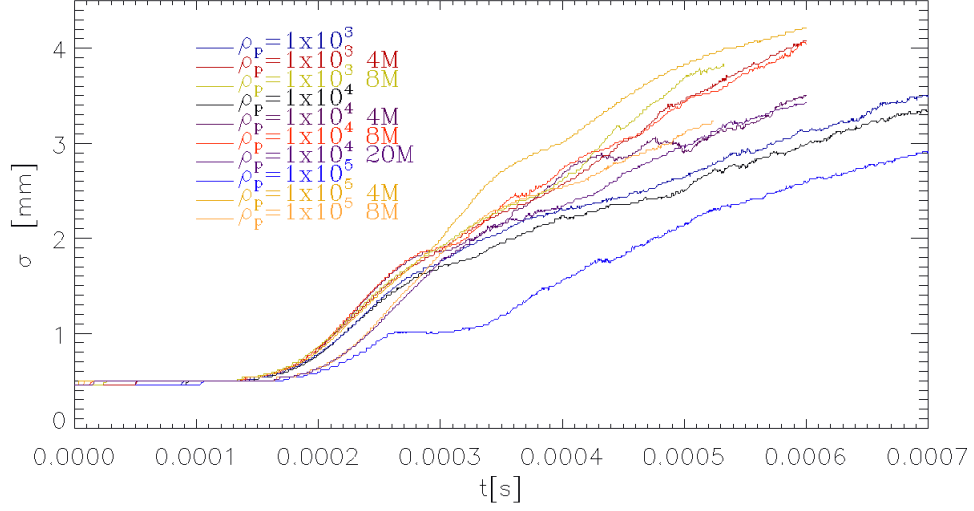


Figure 25: Plot presenting width of particles location within time for 3D case, for all presented densities

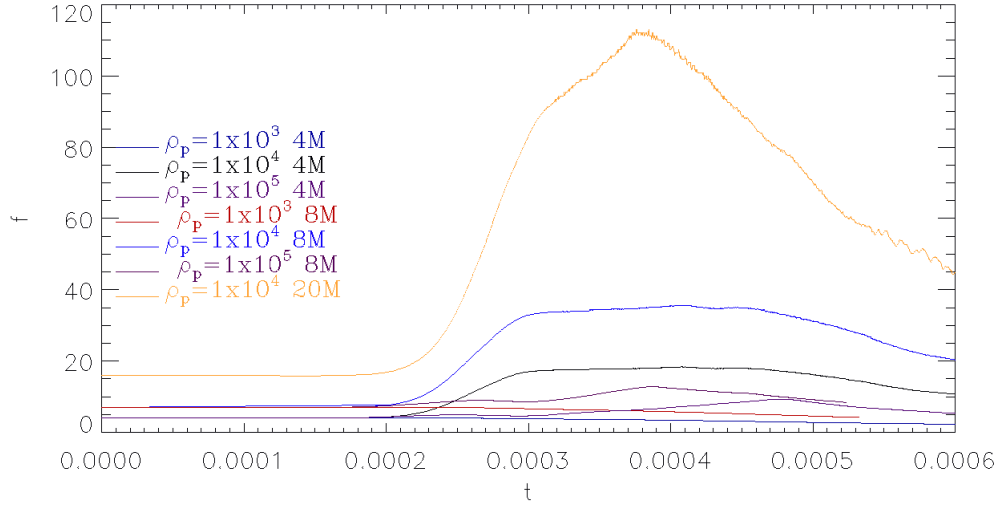


Figure 26: Plot presenting particles clustering for 3D case for different densities and particles amount

The analysis of clustering was done using equation 26, and the results are presented in Fig. 26. Most of the cases seem to be rather shallow. Only those for density  $10^4 \text{ kg/m}^3$  are showing the increase of clusters after 0.0002

seconds - higher values for respectively more particles. On the snapshots in Fig. 20 those clusters are visible on third ones. For 20 million particles, the highest peak is seen around 0.0004s, which is presented in Fig. 20 in the fourth snapshot, and it can be noticed that clusters are the sharpest there.

### 3 Summary

Within the scope of the work, the conversion of solid reacting particles was analyzed in a non-premixed, double shear layer configuration.

It has been clearly shown that a 3D simulation is needed for the tested conditions. The 2D case does not reflect reality accurately enough.

The reaction rate does not change linearly with an increasing number of particles. The reasons for that are clustering and mixing. As the Reynolds number is low, probably mixing is a bigger issue in presented cases. The jet spreading seems to be the fastest for the biggest density, though it is not entirely accurate. The particles are spreading, but are not following the fluid anymore. A longer simulation would show if the tendency of other densities would exceed this.

The tendency to cluster the most is shown in the case with Stokes number equal to 0.35. This can be compared with Graham paper [15], where Reynolds numbers and particles diameters were significantly bigger, though the biggest clusters were seen for Stokes number 0.3. In non-shear cases, the biggest clusters are expected for  $St \approx 1$ .

More work is required to fully understand the process. For example, simulations with a realistic chemistry of the combustion process should be implemented. Another important issue which should be studied in the future work is the case with more particles. Furthermore, particle size distribution and shrinking effect should be included to better represent pulverized coal combustion. What also should be done is comparing results from this thesis with similar simulations done with LES method. That would show if such detailed analyzes are required, or if the difference in results would be small enough to ignore it and simplify calculations.



## References

- [1] Cuenot B., Echehki T., Mastorakos E. *The Flamelet Model for Non-Premixed Combustion* Turbulent Combustion Modeling. Fluid Mechanics and Its Applications, 2011, vol 95. Springer, Dordrecht
- [2] Hawkes Evatt R., Sankaran Ramanan, Sutherland James C., and Chen Jacqueline H., *Scalar mixing in direct numerical simulations of temporally evolving plane jet flames with skeletal CO/H<sub>2</sub> kinetics*, Combustion and Flame, USA, Elsevier Inc., 1540-9489
- [3] Ranga Dinesh K.K. J., Richardson E.S., van Oijen J.A., Luo K.H., Jiang X. *The Scalar Structure of Turbulent Oxy-Fuel Non-Premixed Flames*, ScienceDirect, Energy Procedia 66 2015, 305 – 308
- [4] Krüger Jonas, Haugen Nils Erland L., Mitra Dhrubaditya, Løvås Terese *The effect of turbulent clustering on particle reactivity*, ScienceDirect, Norway, Elsevier Inc., 2016, 2333-2340
- [5] Pitsch H *Improved pollutant predictions in large-eddy simulations of turbulent non-premixed combustion by considering scalar dissipation rate fluctuations*, Proc. Combust. Inst., 29(2):1971–78
- [6] Moin Parviz, Mahesh Krishnan *DIRECT NUMERICAL SIMULATION: A Tool in Turbulence Research*, Annu. Rev. Fluid Mech. 1998. 30:539–78
- [7] Chung T.J. *Computational Fluid Dynamics*, Cambridge University Press, 2002, 0-521-59416-2
- [8] *Pencil Code* <http://www.pencil-code.nordita.org/>, 2017
- [9] Dobler Wolfgang, et. al *The Pencil Code: A High-Order MPI code for MHD Turbulence User's and Reference Manual*, 2017
- [10] Jiang Chiyu *FLUENT - Particles in a Periodic Double Shear Flow* <http://confluence.cornell.edu/display/SIMULATION/FLUENT+-+Particles+in+a+Periodic+Double+Shear+Flow> [02.08.2018]
- [11] Salvi Rodolfo et. al *The Navier-Stokes equations: theory and numerical methods*, Marcel Dekker, Inc. Italy, 2002, 0-8247-0672-2
- [12] Krüger Jonas, Haugen Nils Erland L., Løvås Terese *Correlation effects between turbulence and the conversion rate of pulverized char particles*, Combustion and Flame, Norway, Elsevier Inc., 2017, 0010-2180

- [13] Haugen Nils Erland L., Krüger Jonas, Mitra Dhrubaditya, Løvås Terese *The effect of turbulence on mass transfer rates of small inertial particles with surface reactions*, J. Fluid Mech., pp. 932-951, Cambridge University Press 2017.
- [14] Çengel Yunus A., Cimbala John M. *Fluid Mechanics, fundamentals and applications*, McGraw-Hill, 2006, 0-07-247236-7
- [15] Lau Timothy C. W., Nathan Graham J. *The influence of Stokes number on particle clustering within a two-phase turbulent jet*, The University of Adelaide, Australia, 2015